



Synthesis ZnO Heterostructured Photocatalyst Simulated Solar Irradiation for Carbamazepine Elimination in Aqueous Solution

Eman H. Rdewi* , Ahmed M.H. Abdulkadhim Al-Ghaban , Khalid K. Abbas 

Materials Engineering Dept, University of Technology-Iraq, Alsina'a Street, 10066 Baghdad, Iraq.

*Corresponding author Email: mae.19.19@grad.uotechnology.edu.iq

HIGHLIGHTS

- A ZnO photocatalyst was effectively produced using the sol-gel method and heat treatment.
- The developed ZnO photocatalyst successfully decomposed the CBZ in water under simulated sunlight.
- After 180 minutes, the CBZ compound is degraded with high efficiency of 90% and an absorption capacity of 3.018685664 mg g⁻¹.
- At the 4 pH solution region, the removal effectiveness increased to approximately 95%.

ARTICLE INFO

Handling editor:, Akram R. Jabur

Keywords:

Zinc Oxide
heterostructured nano photocatalyst
Sol-gel
Carbamazepine
solar light.

ABSTRACT

In this study, zinc oxide nanoparticles (ZnO NPs) were produced to photodegrade harmful carbamazepine compounds (CBZ) in water under simulated solar light. The ZnO photocatalyst was prepared in aqueous media using the sol-gel technique with zinc chloride and NaOH as precursors. X-ray diffraction (XRD), Fourier transform infrared spectroscopy (FT-IR), Field Emission Scanning Electron Microscopy (FE-SEM), and ultraviolet-visible diffuse reflectance spectroscopy (UV-vis DRS) were used to characterize the ZnO NPs powder. According to the XRD result, ZnO nanoparticles showed a hexagonal symmetry shape with a 13 nm particle size value. The absorption bands of ZnO nanoparticles were identified using FT-IR spectra peaking. The ZnO nanoparticles produced in this work have a spherical shape, as seen in the FE-SEM picture, with a bandgap of about 3.6 eV, which was determined using the UV-Vis DRS data. The prepared Zinc Oxide heterostructured photocatalyst utilized excellent performance in reducing the Carbamazepine compound with an efficiency of 90%. This study took into account pH solution, catalyst loading, kinetic studies, TOC removal, regeneration, and reusability. The synthesized ZnO successfully removed the Carbamazepine medicine at pH=4. With an R-square of 0.99855, the produced photocatalyst fits well into the pseudo-second-order model. The ZnO heterostructured nano photocatalyst retained its outstanding performance after numerous usage cycles. For these observations, the Zinc Oxide heterostructured photocatalyst for Carbamazepine reduction is a promising photocatalyst.

1. Introduction

Pharmaceuticals, which have been recognized for protecting lives, have been considered a new type of environmental pollutant in recent decades because of their negative impacts on aquatic and human health [1, 3]. Pharmaceutical pollutants emit toxins that can cause some medical problems, are dangerous to human endocrine systems, and effectively make water unfit for drinking and other purposes [4]. For example, some antibiotics were found in potable water treatment facilities in Iraq due to the large number of medicines used by Iraq's public health sector hospitals and care centers [5, 6]. Carbamazepine (CBZ), which is used to treat seizures, trigeminal neuralgia (facial nerve pain), and mental disorders, including bipolar disorder, is one of these antibiotics, mostly found in Asian nations' aquatic environments. However, standard water treatment plants can only remove about 10% of the carbamazepine pollutants from water [7].

The presence of these pollutants in water constitutes a major environmental hazard, and the conventional techniques for wastewater treatment are ineffective in eliminating these pharmaceuticals. As a result, developing and implementing removal methods for these emerging contaminants is important [8, 10]. Therefore several physical-chemical techniques such as adsorption [11], filtration [12], and membrane bioreactor (reverse osmosis) [13] have been applied for wastewater treatment. However, advanced oxidation processes (AOPs) are more effective in eliminating pollution than other treatments that only

carry contamination from one state to another [14]. Photocatalysis is one of the most important processes in AOPs, which involves heterogeneous and homogeneous photocatalysis based on sunlight, electrolysis, ozone, Fenton detector, and ultrasound [15, 16]. Photocatalysis has emerged as a research topic as a clean and renewable technology with a high ability to resolve environmental problems [17]. And the studies on photocatalytic degradation of pharmaceuticals illustrated that photocatalysis is an assured technology to shorten the influence of these compounds, even when pharmaceuticals are displayed in small amounts. Moreover, the probability of applied solar light enhances the activity of this process [11]. Heterogeneous photocatalysis is a bright process, especially in power and environmental industries [11,13]. Zinc oxide (ZnO) is believed to be a more efficient heterogeneous photocatalyst owing to its distinctive electrical and optical characteristics, such as a wide bandgap with a 3.37 eV value [18]. In addition, ZnO has around 60 meV binding energy, good optical transparency, excellent electron mobility, and photo-stability [19,21]. These features have been relevant in various applications, including photocatalysis, solar cells, sensors, and medicine. Particle size is crucial for many industries, and numerous research studies are actively investigating ZnO nanoparticles [20,23]. Nanoparticles have incredible physical and chemical characteristics because of their high surface area to volume ratio and the availability of infinite grains that occupy higher concentration defects [24-28].

Consequently, photocatalysis employing nanostructure ZnO is more efficient than bulk ZnO. ZnO nanoparticles have been produced using various methods, including precipitation method, combustion, hydrothermal method, micro-emulsion, chemical bath deposition, sol-gel, and spray pyrolysis methods [20,23, 29, 30]. The particle size and shape of the produced ZnO nanoparticles are influenced by the solvents, temperature, and experiment medium [12]. The sol-gel process is preferred for ZnO nanostructure synthesis due to its low production costs, excellent performance, repeatability, lower temperature method, ease of controlling physical attributes, good composition stability, and optical quality [31, 32].

For this study, Sodium hydroxide was used to make Zinc Oxide photocatalyst using the sol-gel method with only water as a solvent. This photocatalyst was then used to remove Carbamazepine from water.

2. Materials and Methods

2.1 Materials

Carbamazepine pharmaceuticals are synthesized by Novartis India Co., Ltd. Acetonitrile HPLC grade from Alpha Chemika. ZnCl_2 (min. 97%) was produced by Avonchem Co., Ltd. NaOH (min.99%) and ethanol (min. 99.9%) were synthesized by the Scharlab S.L. group, and distilled and deionized water for ZnO NPs production.

2.2 Synthesis of ZnO NPs

To prepare a ZnO heterostructured photocatalyst using the sol-gel process, follow these steps (Fig.1.): Firstly, 10 g of sodium hydroxide (NaOH) was added to 100 mL of distilled water, and the solution temperature was elevated to 90°C with constant stirring. Secondly, when reaching the required temperature, 17 g of zinc chloride was soluble in 100 mL of distilled water and put drop by drop into the NaOH solution for 60 min. When ZnCl_2 is dripped into an aqueous alkaline solution, ZnO precipitates immediately. Moreover, the coloring shifts from translucent to milky color. The mixture was swirled for roughly 2 hours after the dropping process to obtain the appropriate temperature. Then the resulting mixture was filtered and washed five times to ensure that all NaCl was removed. Next, ethanol was used to peptize the purified particles in an ultrasonic device at 50°C for 15 minutes to destroy micro-agglomeration and reach nano units from bulk suspensions. Finally, the particles were filtered and washed multiple times in a vacuum pump device by dissolving them in de-ionized water before drying at 70°C for six h.

2.3 Characterizations

Field emission scanning electron microscopy (FE-SEM) was used to study the morphology of a heterostructured ZnO nano photocatalyst. An X-ray diffractometer (XRD, Angstrom Advanced Inc.) Model ADX 2700 with Cu-K radiation was used to evaluate the crystallographic data. The Fourier transform infrared spectra (FTIR, Bruker tensor 27) was employed to inspect ZnO nanostructured in the 400 cm^{-1} to 4000 cm^{-1} wavelength range. In addition, the ultraviolet-visible diffuse reflectance spectroscopy (UV-vis DRS) was used to study the absorption spectra with the optical band gap energy of ZnO nanoparticles using a Shimadzu UV-3600 UV/vis spectrophotometer.

High-performance liquid chromatography (HPLC) from Kinetex, Phenomenex Co., AUS was used to evaluate carbamazepine pharmaceutical (CBZ) quantity, utilizing a Varian Prostar 210 chromatographic system using a UV spectrophotometer (20 SBD, 270 nm) and a C18 reversed-phase column (5 m, 4.6 250 mm). In this research, two mobility phases were used. The A solution contains 70% methanol and 30% water, whereas the solution (B) contains HPLC-grade acetonitrile. The flow rate is 0.7 mL min^{-1} with a 10-minute duration. The technique described here is based on earlier research [33]. Shimadzu's TOC-VCPH analyzer detects total organic carbon (TOC) and impurities within samples taken. The photocatalyst solutions were filtered using 0.45 μm filtration paper before the HPLC and TOC experiments. All of the trials were carried out at a temperature of 25 °C.

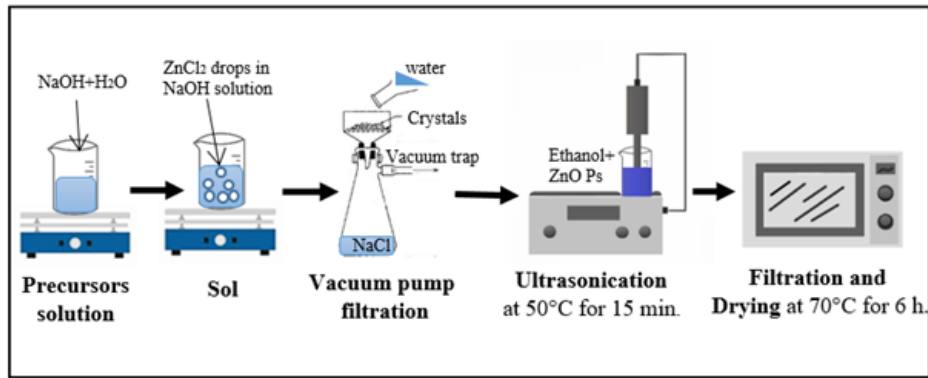


Figure 1: Schematic diagram illustrating the steps in the preparation of ZnO NPs Analysis Methods

2.4 The photocatalytic activity

In a typical procedure, the photocatalytic activities of the ZnO nano-heterostructural photocatalyst to remove Carbamazepine (CBZ) pharmaceutical from water are investigated under solar light irradiation. The equipment used in this process is a halogenate high-pressure lamp JTT-150 W with a 100 mW/cm^2 luminous intensity and a beaker jacket with a 500 mL capacity. 10 mg L^{-1} of ZnO photocatalyst was used, according to the previous work [34]. Then the photocatalyst was mixed with the initial concentration of the Carbamazepine pharmaceutical was $5 \text{ ppm (mg L}^{-1})$ at ambient temperature. The pH solution effectiveness on the removal efficiency of CBZ was indicated at 2.0, 4.0, 6.0, 7.0, and 8.0 pH. Next, a portion of the ZnO heterostructured photocatalyst is put in the photocatalytic reactor with a predetermined concentration of Carbamazepine in the dark with continuous stirring. For 60 minutes, each experiment runs for 180 minutes under simulated sunlight, with a syringe sample being obtained every 30 minutes. To determine the quantification of CBZ at different irradiation times, an HPLC analysis of the filtrated sample was carried out. The photocatalyst that remained in the water samples was removed using a Whatman filter paper size of 2.5 m before further testing. The residual pharmaceutical concentrations were obtained by calculating the area under the curve. The removal efficiency of CBZ was calculated using Eq. (1) [34]:

$$\eta(\%) = \frac{C_i - C_f}{C_i} \times 100 \quad (1)$$

Where η is the photodegradation efficiency, C_i is the initial concentration of the Carbamazepine compound, and C_f is the final concentration of the pharmaceutical.

3. Results and Discussion

3.1 X-ray diffraction (XRD)

X-ray diffraction (XRD) was applied to study the crystallographic properties of ZnO nanopowder, as shown in Fig. 2. The diffraction peaks at $31.84, 34.50, 36.30, 47.56, 56.65, 62.90, 66.49^\circ, 67.95^\circ, 69.15, 72.61, 77.05^\circ, 81.49^\circ,$ and 89.7° have been precisely identified as hexagonal wurtzite phases of ZnO (JPCDS card number: 36-1451). Other than the wurtzite phase of the ZnO nanoparticles, there are no identifiable peaks of impurity phases, demonstrating that the sample is crystalline. Furthermore, the average crystal size of the synthesized photocatalyst is 13 nm, which is lower than the ZnO nanoparticles generated in the previous works, which ranged from 41 nm to 29 nm for the first work [35], and 25.39 nm to 33.6 nm for the other work [36]. The average crystal size of the ZnO NPs was determined according to the Debye-Scherrer equation by Eq. (2) [37]:

$$D = \frac{K\lambda}{\beta \cos \theta} \quad (2)$$

Where D = crystal size of ZnO NPs, K = a constant of 0.94, λ = the X-ray wavelength, β = the half peak width, and θ = the diffraction angle.

3.2 Field emission scanning electron microscopy (FE-SEM)

The shape of the resulting powder was studied using Field Emission Scanning Electron Microscopy (FE-SEM). In figure 3, FE-SEM pictures of ZnO NPs at different magnifications. These images demonstrate the formation of ZnO nanoparticles. These nanoparticles are roughly sphere-shaped, and many of them contain some faceting, as shown in the photos. The high surface energy of ZnO NPs caused some aggregation in the ZnO structure, resulting in the development of bulk structures with reduced reactivity [38].

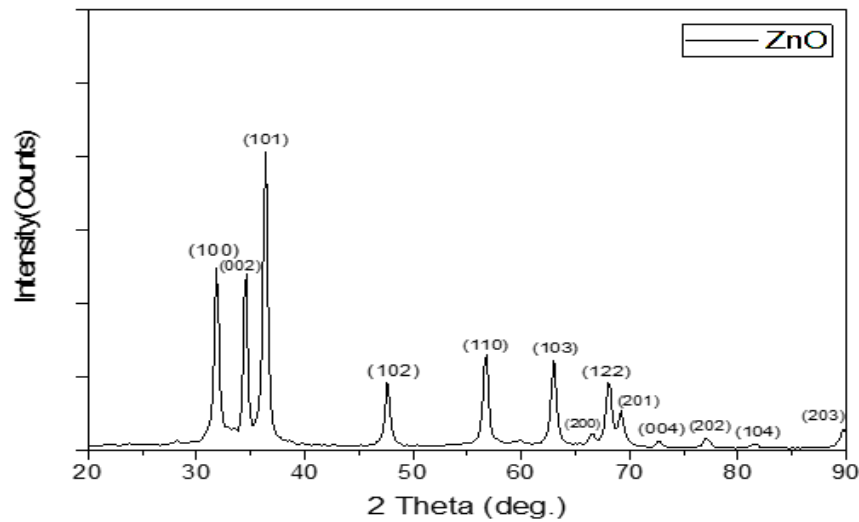


Figure 2: X-ray diffraction results of the produced ZnO NPs

3.3 Fourier transform infrared spectroscopy (FT-IR)

The FT-IR spectra of Zinc Oxide (ZnO) nano-size were measured in Fig. 4. Figure 4 shows that the stretching vibration of Zn-O is responsible for the distinctive bands of 437 cm^{-1} , 547 cm^{-1} , and 406 cm^{-1} in the lower energy range [39]. Due to atmospheric moisture and CO_2 , the stretching vibration mode of C=O and C-O residues is defined as three different bands at 1658 cm^{-1} , 1545 cm^{-1} , and 1449 cm^{-1} . The O-H bending vibration of physisorbed water is responsible for the peak at 3273 cm^{-1} .

3.4 Ultraviolet-visible diffuse reflectance spectroscopy (UV-vis DRS)

Ultraviolet-visible diffuse reflectance spectroscopy (UV-vis DRS) was used to examine the optical absorption properties of Zinc Oxide nanoparticles (Fig.5). The Tauc relation was used to calculate the optical band gap of ZnO NPs as utilized in (Eq.3) [40]:

$$\alpha h\nu = A^*(h\nu - E_g) \quad (3)$$

Where A = constant, $h\nu$ = input photon energy, α = optical absorption coefficient, E_g = material's energy bandgap, and $n = 1/2$ is the exponent for direct bandgap and dipole-allowed transitions.

Plotting $(h\nu)^2$ against $h\nu$ and extrapolating the linear component of the absorption edge to locate the intersection with the energy axis yields the energy bandgap for ZnO nanoparticles (as shown in Fig. 5). Consequently, ZnO nanopowder has a strong absorption band of about 300 nm (Fig.5 a), with a bandgap of 3.6 eV for ZnO (Fig. 5 b). A conclusion should point out the distinguished results of the achieved work and not replicate the abstract. A conclusion may suggest recommendations for work extension and new applications. [37]. The FTIR data of the synthesized ZnO NPs indicated their preparation had been successfully achieved.

3.5 Photodegradation activity

3.5.1 Removal pharmaceutical Carbamazepine

The removal performance of the Carbamazepine compound (CBZ) was studied under optimal circumstances using the produced ZnO photocatalyst. The photocatalysis impact of the CBZ was studied, shown in Figure 6. Before being exposed to the simulated sunlight, 10 mg mL^{-1} of the heterostructured photocatalyst was placed in the photocatalytic reactor with 5 mg L^{-1} of pharmaceutical for a sample was run in the dark for 60 minutes, followed by 180 minutes under solar light. Under simulated solar light irradiation, the CBZ compound was highly absorbed on the surface of the ZnO nano photocatalyst, with an absorption rate of more than 70% in the first 30 minutes. While the decomposition efficiencies of CBZ compound in darkness were less than 20% when using the ZnO photocatalyst. The photodecomposition of the Carbamazepine compound by ZnO nano heterostructured was increased progressively with time when exposed to the solar irradiation to be about 80% after one hour. The ZnO NPs photocatalyst indicates a strong pharmaceutical removal reaching 90 percent, which attributable to a reduction in the ZnO nano heterostructured particle size and solar light irradiation.

3.5.2 pH solutions:

The pH solutions have a considerable effect and are a critical part of the photodegradation process of the pharmaceutical compounds [41]. The impact of pH solution on ZnO heterostructured nano photocatalyst was examined in this work. Various pH solutions were made at 2, 4, 6, 7, and 8 using 0.1M NaOH & 0.1M HCl solutions as utilized in figure 7. At 8 and 2 PH regions, the photodegradation performance of carbamazepine antibiotics was 75 and 80 percent, respectively. The removal

effectiveness increased in the neutral and 4 pH solution regions to about 90% removal efficiency at 7 PH solution. The CBZ photodegradation achieved an outstanding performance of 95% at a 4 pH solution (Fig.7).

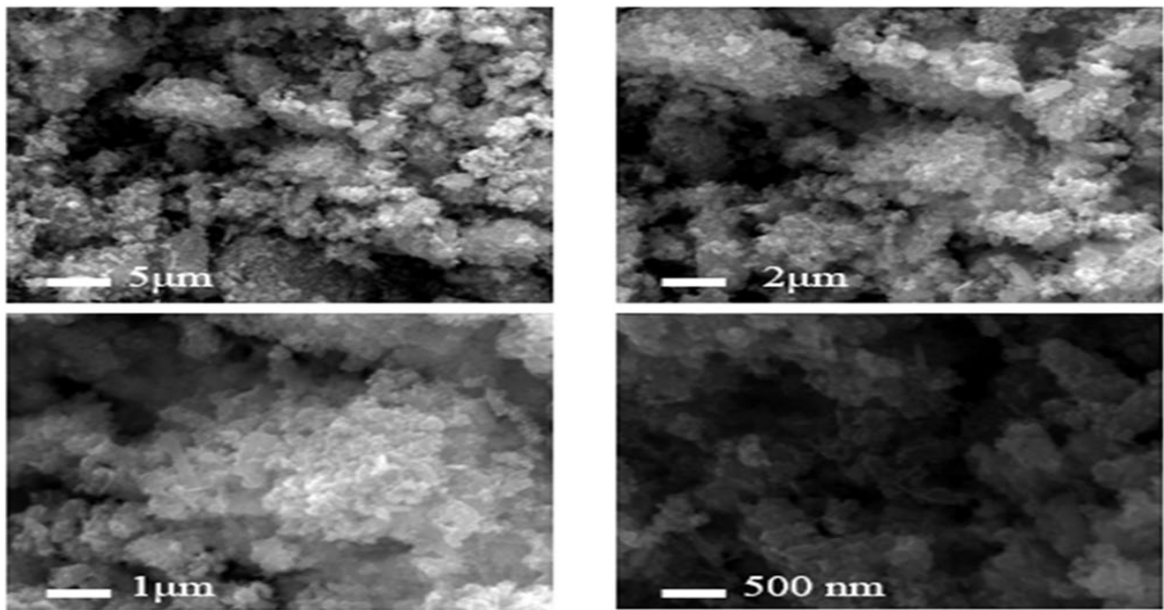


Figure 3: FE-SEM images of ZnO nanoparticles at various magnifications

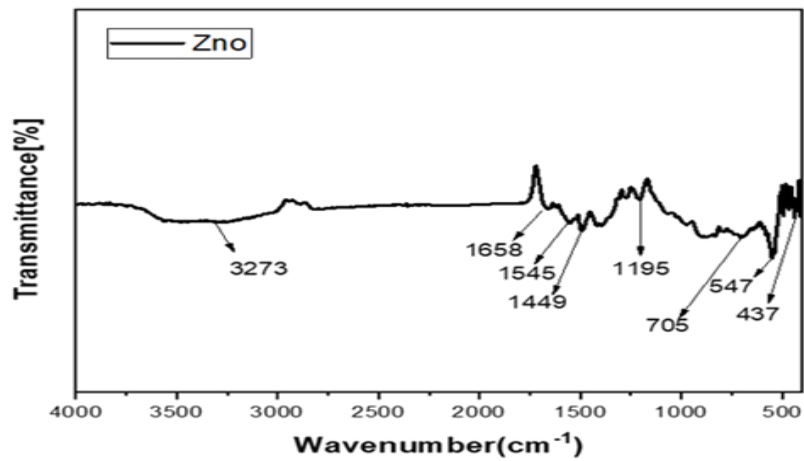


Figure 4: FTIR of ZnO nanoparticles

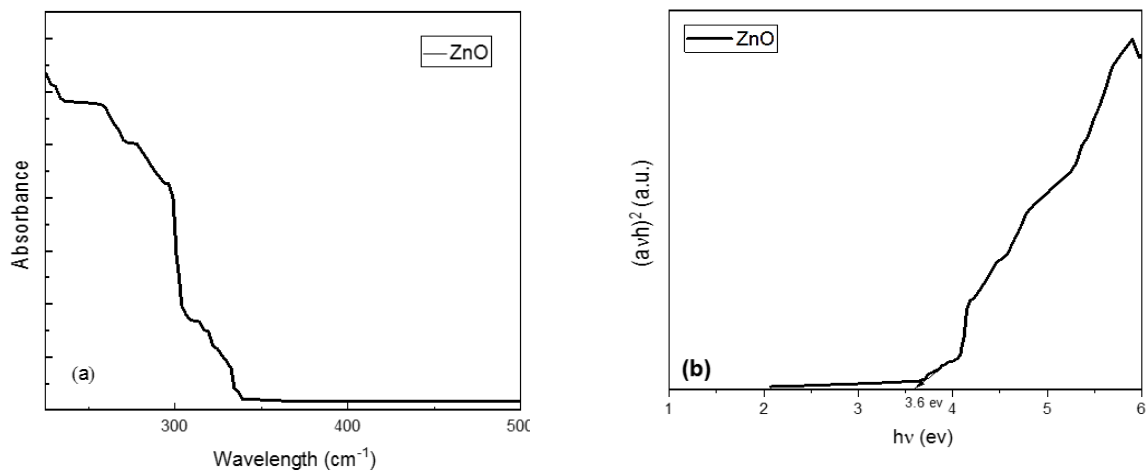


Figure 5: (a) UV-vis diffused absorption spectra of ZnO nano photo catalyst, (b) Band gap energy of ZnO nano photo catalyst

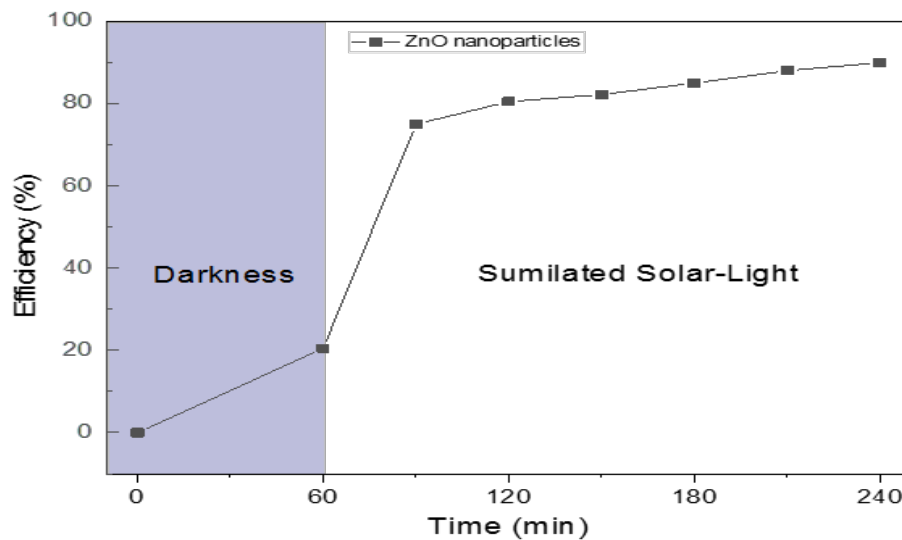


Figure 6: The Carbamazepine compound's photo degradation effectiveness under the following conditions: 5 mg L⁻¹ CBZ, 10 g L⁻¹ ZnO nano photo catalyst, pH solution =7

3.5.3 Kinetic study

Whether homogeneous or heterogeneous, the photocatalyst kind has a significant impact on the advanced oxidation process's performance. The heterogeneous photocatalysts are preferred because they have high electron mobility on their surface, which reduces recombination rate performance [42]. To analyze the behavior of kinetic photodecomposition, the Pseudo first and second models were examined [43]. The better-suited model was selected by the highest correlation coefficient (R-square). The first order pseudo kinetic model described in Eq. (4):

$$\ln(C_o/C_f) = k_{app} t \quad (4)$$

Where C_o is the Carbamazepine compound initial concentration in mg/L, C_f is the final Carbamazepine compound concentration in mg/L, k_{app} is a Pseudo-first order constant in min⁻¹, and t is the photocatalytic reaction time (min). As utilized in Fig.8, the plotting of $\ln(C_o/C_f)$ versus t at optimum conditions obtains the rate constant (k_{app}) was 0.01028 min⁻¹. While the R-square of the pseudo-first-order was determined to be 0.76735 (Fig.8 a). The Pseudo second-order kinetic model described in Eq. (5)

$$\frac{t}{q_t} = \frac{1}{k_2} q_e^2 + \frac{1}{q_e} t \quad (5)$$

Where q_t is the photodegraded pharmaceutical quantity (mg/g), k_2 is the Pseudo-second order constant (g mg⁻¹ min⁻¹), q_e is the degradation capacity at equilibrium conditions, and t is a photodegradation time in min. The k_2 value is 0.064029671 g mg⁻¹ min⁻¹, and the R-square value of the Pseudo second order is 0.99855, derived by the plotting of t/q_t Vs. t . In addition, the maximal absorption capacity of Carbamazepine is 3.018685664 mg g⁻¹(Fig. 8b). Therefore, the results show that the ZnO photocatalyst corresponds to the pseudo second model, owning the greatest coefficient of correlation value in the pseudo second order compared to its value in the pseudo-first order model under optimal situations.

3.5.4 Total organic carbon removal activity (TOC)

The total removal of organic carbon compounds was examined under optimal conditions utilizing a ZnO photocatalyst, as appears in Figure 9. Total organic compound removal effectiveness was greater than 50% in the first 30 minutes. And this TOC removal efficiency improved with time to approximately 70% after 90 minutes. The degradation of ZnO NPs at 120 and 140 minutes shows an 85% and 88% rise, respectively. The highest degradation of the organic carbon was indicated at 180 minutes to reach 90%. The inclusion of ZnO improved the removal effectiveness of the pharmaceutical drug. Moreover, the heterostructured photocatalyst achieved nearly full breakdown of the carbamazepine molecule and hazardous organic materials from water samples.

3.5.5 Regeneration and usability

The multi-use of ZnO photocatalyst samples was studied to demonstrate the catalyst's capacity to function for extended periods under appropriate circumstances. The efficiency of Carbamazepine (CBZ) degradation was investigated over eight cycles, as shown in Fig.10. After each cycle, the ZnO heterostructural nano-photocatalyst was filtered and washed with 50% deionized water and 50% ethanol. Afterward, the photocatalyst sample was dried in an oven at 70 °C for 4 hours. In the eighth cycle, the photodecomposition of the CBZ compound exhibited a slight decrease (less than 10%) in photocatalytic efficiency. It is worth noting that until the fifth cycle, photodegradation of the CBZ compound occupied less than 2% of the performance in CBZ reduction. After that, the removal efficiency dropped, reaching 82 percent during the eighth cycle. This restriction in

photo degradation results from the potential of intermediary molecules interfering with the degradation mechanism, decreasing the redox reaction.

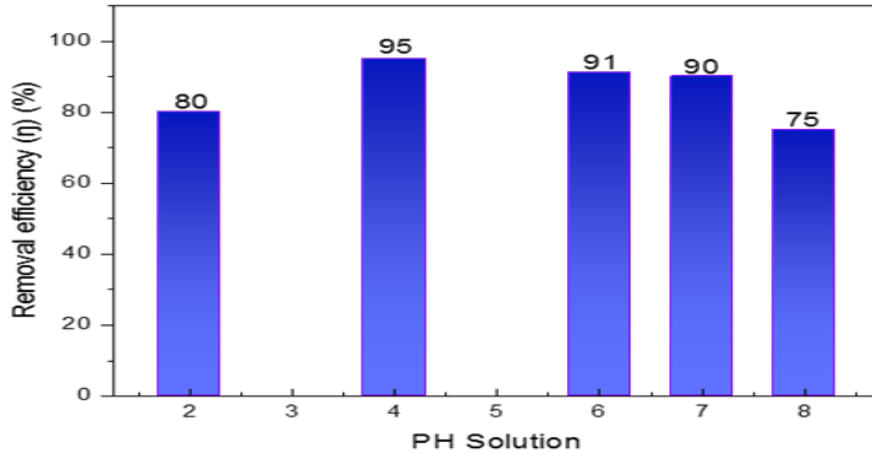


Figure 7: Carbamazepine efficiency at varied pH levels using ZnO nano photo catalyst at the following conditions: 5 mg L⁻¹ CBZ, 10 g L⁻¹ ZnO photo catalyst

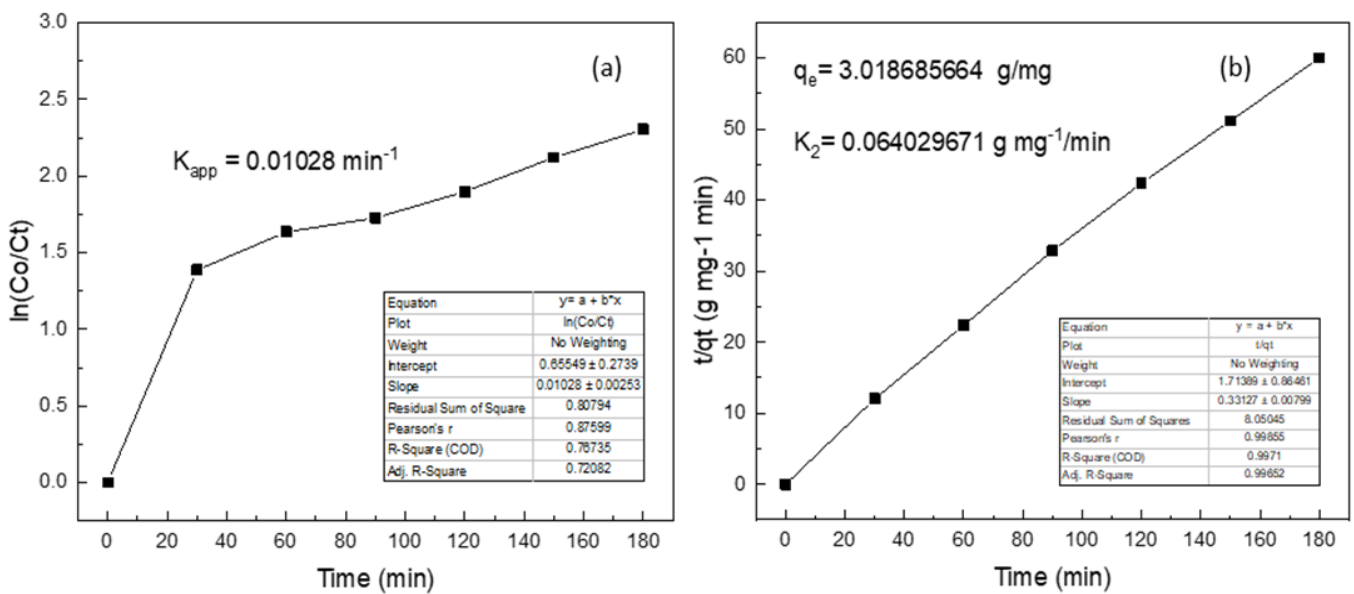


Figure 8: Carbamazepine efficiency at varied pH levels using ZnO nano photocatalyst at the following conditions: 5 mg L⁻¹ CBZ, 10 g L⁻¹ ZnO photocatalyst

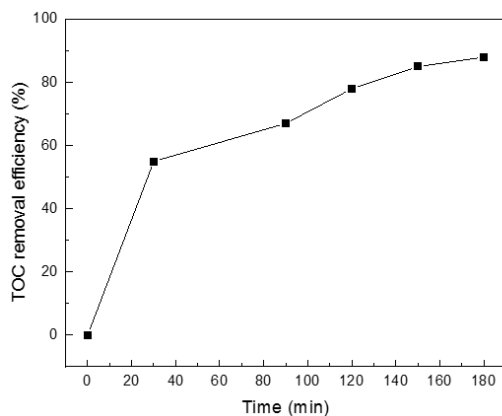


Figure 9: The total removal of organic compounds using ZnO nano heterostructured at 5 mg L⁻¹ Carbamazepine compound, 10 g L⁻¹, pH solution = 7

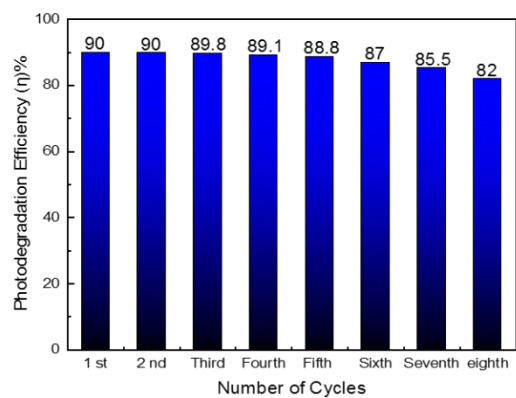


Figure 10: The reusability of the ZnO heterostructured nano photo catalyst after eight Cycles of the treatment process

4. Conclusion

ZnO NPs heterostructured crystalline structure photocatalyst was produced by performing the sol-gel method, using ZnCl_2 and NaOH at 90°C at a dripping time of 60 min. This resulted in a small crystalline size of 13 nm, further characterized by XRD, SEM, UV-vis diffuse reflectance spectra (DRS), and FTIR. XRD and SEM results demonstrate the nano heterostructured shape of a ZnO photocatalyst. Furthermore, the degradation of the CBZ compound at high efficiency is 90% when using ZnO photocatalyst after 180 min. The photodegradation performance of the heterostructured nano photocatalyst in a natural medium and at a 4 PH solution was excellent. After 8 cycles, the nano heterostructured ZnO was investigated and significantly influenced its performance. The results ensure the use of ZnO nanoparticles for CBZ removal from the water.

Acknowledgment

The authors would like to express their pleasure to the Department of Materials Engineering at Baghdad's University of Technology Iraq. The authors would also like to thank the anonymous reviewers and the editor for their useful suggestions and insightful comments.

Author contribution

All authors contributed equally to this work.

Funding

This research received no specific grant from any funding agency in the public, commercial, or not-for-profit sectors.

Data availability statement

The data that support the findings of this study are available on request from the corresponding author.

Conflicts of interest

The authors declare that there is no conflict of interest.

References

- [1] M. Patel, R. Kumar, K. Kishor, M. S. T., Pittman Jr, C. U., & Mohan, D. Pharmaceuticals of emerging concern in aquatic systems: chemistry, occurrence, effects, and removal methods, *Chem. Rev.*, 119 (2019) 3510-3673. <https://doi.org/10.1021/acs.chemrev.8b00299>
- [2] N. Bortey-Sam, S. M. Nakayama, Y. Ikenaka, O. Akoto, E. Baidoo, H. Mizukawa, & M. Ishizuka, Health risk assessment of heavy metals and metalloid in drinking water from communities near gold mines in Tarkwa, Ghana. *Environ. Monit. Assess.*, 18 (2015) 1-12. <https://doi.org/10.1007/s10661-015-4630-3>
- [3] M. Hanna-Attisha, J. LaChance, R. C. Sadler, & A. C. Schnepf, Elevated blood lead levels in children associated with the Flint drinking water crisis: a spatial analysis of risk and public health response, *Am. J. Public Health* ., 106 (2016) 283-290. <https://doi.org/10.2105%2FAJPH.2015.303003>
- [4] R. Das, Application photocatalysis for treatment of industrial waste water—a short review, *Open Access Library J.*, 1 (2014) 1-17. <https://doi.10.4236/oalib.1100713>.
- [5] O. S. Al-Khazraji, & A. B. Boxall, Risk-based prioritization of pharmaceuticals in the natural environment in Iraq, *Environ. Sci. Pollut. Res.*, 23 (2016) 15712-15726. <https://doi.org/10.1007/s11356-016-6679-0>
- [6] A. R. Mahmood, H. H. Al-Haideri, & F. M. Hassan, Detection of antibiotics in drinking water treatment plants in Baghdad City, Iraq, *Adv. public health* ., (2019). <https://doi.org/10.1155/2019/7851354>
- [7] A. Carabin, P. Drogui, & D. Robert, Photo-degradation of Carbamazepine using TiO_2 suspended photocatalysts, *J. Taiwan Inst. Chem. Eng.*, 54 (2015) 109-117. <https://doi.org/10.1016/j.jtice.2015.03.006>
- [8] S. Majumder, S. Chatterjee, P. Basnet, & J. Mukherjee, ZnO based Nanomaterials for Photocatalytic degradation of Aqueous Pharmaceutical Waste Solutions—A Contemporary Review, *Environ. Nanotechnol. Monit. Manag.*, (2020) 100386. <https://doi.org/10.1016/j.enmm.2020.100386>
- [9] A. Mirzaei, Z. Chen, F. Haghghat, & L. Yerushalmi, Removal of pharmaceuticals and endocrine disrupting compounds from water by zinc oxide-based photocatalytic degradation: a review, *Sustain. Cities Soc.*, 27 (2016) 407-418. <https://doi.org/10.1016/j.scs.2016.08.004>
- [10] J. O. Tijani, O. O. Fatoba, & L. F. Petrik, A review of pharmaceuticals and endocrine-disrupting compounds: sources, effects, removal, and detections, *Water Air Soil Pollut.*, 224 (2013) 1-29. <http://dx.doi.org/10.1007/s11270-013-1770-3>
- [11] A. Mirzaei, A. Ebadi, & P. Khajavi, Kinetic and equilibrium modeling of single and binary adsorption of methyl tert-butyl ether (MTBE) and tert-butyl alcohol (TBA) onto nano-perfluorooctyl alumina, *Chem. Eng. J.*, 231 (2013) 550-560. <http://dx.doi.org/10.1016%2Fj.cej.2013.07.017>

- [12] P. M. Bradley, L. B. Barber, J. W. Duris, W. T. Foreman, E. T. Furlong, L. E. Hubbard, & D. W. Kolpin, Riverbank filtration potential of pharmaceuticals in a wastewater-impacted stream, *Environ. Pollut.*, 193 (2014) 173-180. <https://doi.org/10.1016/j.envpol.2014.06.028>
- [13] D. Dolar, M. Gros, S. Rodriguez-Mozaz, J. Moreno, J. Comas, I. Rodriguez-Roda, & D. Barceló, Removal of emerging contaminants from municipal wastewater with an integrated membrane system, MBR-RO, *J. Hazard. Mater.*, 239 (2012) 64-69. <https://doi.org/10.1016/j.jhazmat.2012.03.029>
- [14] E. S. Elmolla, & M. Chaudhuri, Comparison of different advanced oxidation processes for treatment of antibiotic aqueous solution, *Desalination.*, 256 (2010) 43-47. <https://doi.org/10.1016/j.desal.2010.02.019>
- [15] M. Klavarioti, D. Mantzavinos, & D. Kassinos, Removal of residual pharmaceuticals from aqueous systems by advanced oxidation processes, *Environ. Int.*, 35 (2009) 402-417. <https://doi.org/10.1016/j.envint.2008.07.009>
- [16] M., Samadi, M. Zirak, A. Naseri, E. Khorashadizade, & A. Z. Moshfegh, Recent progress on doped ZnO nanostructures for visible-light photocatalysis., *Thin Solid Films.*, 605 (2016) 2-19. <https://doi.org/10.1016/j.tsf.2015.12.064>
- [17] Y. Fu, Z. Li, Q. Liu, X. Yang, & H. Tang, Construction of carbon nitride and MoS₂ quantum dot 2D/0D hybrid photocatalyst: direct Z-scheme mechanism for improved photocatalytic activity, *Chin. J. Catal.*, 38 (2017) 2160-2170. [https://doi.org/10.1016/S1872-2067\(17\)62911-5](https://doi.org/10.1016/S1872-2067(17)62911-5)
- [18] D. Vogel, P. Krüger, & J. Pollmann, Ab initio electronic-structure calculations for II-VI semiconductors using self-interaction-corrected pseudopotentials, *Phys. Rev. B.*, 52 (1995) R14316. <https://doi.org/10.1103/PhysRevB.52.R14316>
- [19] C. Tian, Q. Zhang, A. Wu, M. Jiang, Z. Liang, B. Jiang, & H. Fu, Cost-effective large-scale synthesis of ZnO photocatalyst with excellent performance for dye photodegradation, *Chem. Commun.*, 48 (2012) 2858-2860. <https://doi.org/10.1039/C2CC16434E>
- [20] J. Ungula, & B. F. Dejene, Effect of solvent medium on the structural, morphological and optical properties of ZnO nanoparticles synthesized by the sol-gel method, *Phys. B: Condens. Matter.*, 480 (2016) 26-30. <https://doi.org/10.1016/j.physb.2015.10.007>
- [21] H. R. Ghorbani, F. P. Mehr, H. Pazoki, & B. M. Rahmani, Synthesis of ZnO nanoparticles by precipitation method, *Orient. J. Chem.*, 31 (2015) 1219-1221. <http://dx.doi.org/10.13005/ojc/310281>
- [22] S. S. Kulkarni, & M. D. Shirsat, Optical and structural properties of zinc oxide nanoparticles, *Int. J. Curr. Adv. Res.*, 2 (2015) 14-18.
- [23] S. S. Kumar, P. Venkateswarlu, V. R. Rao, & G. N. Rao, Synthesis, characterization and optical properties of zinc oxide nanoparticles, *Int. Nano Lett.*, 3 (2013) 1-6. <https://doi.org/10.1186/2228-5326-3-30>
- [24] P. Majzlíková, J. Sedláček, J. Prášek, J. Pekárek, V. Svatoš, A. G. Bannov, & J. Hubálek, Sensing properties of multiwalled carbon nanotubes grown in MW plasma torch: Electronic and electrochemical behavior, gas sensing, field emission, IR absorption, *Sensors*, 15 (2015) 2644-2661. <https://doi.org/10.3390/s150202644>
- [25] F. Maglia, I. G. Tredici, & U. Anselmi-Tamburini, Densification and properties of bulk nanocrystalline functional ceramics with grain size below 50 nm, *J. Eur. Ceram. Soc.*, 33(2013)1045-1066. <http://dx.doi.org/10.1016%2Fj.jeurceramsoc.2012.12.004>
- [26] D. H. Kim, Effects of phase and morphology on the electrochromic performance of tungsten oxide nano-urchins, *Sol. Energy Mater. Sol. Cells.*, 107 (2012) 81-86. <https://doi.org/10.1016/j.solmat.2012.07.030>
- [27] S. P. Jiang, Nano scale and nanostructured electrodes of solid oxide fuel cells by infiltration: advances and challenges, *Int. J. Hydrogen Energy.*, 37 (2012) 449-470. <https://doi.org/10.1016/j.ijhydene.2011.09.067>
- [28] J. Jeevanandam, A. Barhoum, Y. S. Chan, A. Dufresne, & M. K. Danquah, Review on nanoparticles and nanostructured materials: history, sources, toxicity and regulations, *Beilstein J. Nanotechnol.*, 9 (2018) 1050-1074. <https://doi.org/10.3762/bjnano.9.98>
- [29] G. Amin, M. H. Asif, A. Zainelabdin, S. Zaman, O. Nur, & M. Willander, Influence of pH, precursor concentration, growth time, and temperature on the morphology of ZnO nanostructures grown by the hydrothermal method, *J. Nanomater.*, 2011. <https://doi.org/10.1155/2011/269692>
- [30] J. Guo, & C. Peng, Synthesis of ZnO nanoparticles with a novel combustion method and their C₂H₅OH gas sensing properties, *Ceram. Int.*, 41 (2015) 2180-2186. <http://dx.doi.org/10.1016/j.ceramint.2014.10.017>
- [31] M. Vafae, & M. S. Ghamsari, Preparation and characterization of ZnO nanoparticles by a novel sol-gel route, *Mater. Lett.*, 61 (2007) 3265-3268. <https://doi.org/10.1016/j.matlet.2006.11.089>
- [32] H. Köse, Ş. Karaal, A. O. Aydın, & H. Akbulut, A facile synthesis of zinc oxide/multiwalled carbon nanotube nanocomposite lithium ion battery anodes by sol-gel method, *J. Power Sources*, 295 (2015) 235-245. <https://doi.org/10.1016/j.jpowsour.2015.06.135>

- [33] R. G. Kelmann, G. Kuminek, H. F. Teixeira, & L. S. Koester, Determination of carbamazepine in parenteral nanoemulsions: development and validation of an HPLC method, *Chromatographia*, 66 (2007) 427-430. <http://dx.doi.org/10.1365%2Fs10337-007-0314-7>
- [34] M. A. Bhatti, A. A. Shah, K. F. Almani, A. Tahira, S. E. Chalanger, A. dad Chandio, & Ibupoto, Z. H. Efficient photo catalysts based on silver doped ZnO nanorods for the photo degradation of methyl orange, *Ceram. Int.*, 45 (2019) 23289-23297. <https://doi.org/10.1016/j.ceramint.2019.08.027>
- [35] G. S Jaber, K. S .Khashan, & M. J Abbas, Preparation ZnO nanoparticles with Different Concentration by Laser Ablation in Liquid, *Eng. Technol. J.*, 39 (2021) 197-202. <https://doi.org/10.30684/etj.v39i1B.1880>
- [36] T. A. Hassan, A. M. Ali, & A. Qassim, Nano rods and flowerlike synthesis by hydrothermal growth method without catalysts, *Eng. Technol. J.*, (2015) 33.
- [37] B.D. Cullity, *Elements of X-ray Diffraction*. Addison-Wesley Publishing; 1956.
- [38] R. Hong, T. Pan, J. Qian, & H. Li, Synthesis and surface modification of ZnO nanoparticles, *Chem. Eng. J.*, 119 (2006) 71-81. <https://doi.org/10.1016/j.cej.2006.03.003>
- [39] H. Kleinwechter, C. Janzen, J. Knipping, H. Wiggers, & P. Roth, Formation and properties of ZnO nano-particles from gas phase synthesis processes, *J. Mater. Sci.*, 37 (2002) 4349-4360. <https://doi.org/10.1023/A:1020656620050>
- [40] J. Tauc, R. Grigorovici, & A. Vancu, Optical properties and electronic structure of amorphous germanium, *Phys. Status Solidi B.*, 15 (1966) 627-637. <http://dx.doi.org/10.1002/pssb.19660150224>
- [41] M. Qamar, & M. Muneer, A comparative photocatalytic activity of titanium dioxide and zinc oxide by investigating the degradation of vanillin, *Desalination*, 249 (2009) 535-540. <https://doi.org/10.1016/j.desal.2009.01.022>
- [42] C. McManamon, J. D. Holmes, & M. A. Morris, Improved photocatalytic degradation rates of phenol achieved using novel porous ZrO₂-doped TiO₂ nanoparticulate powders, *J. Hazard. Mater.*, 193 (2011) 120-127. <https://doi.org/10.1016/j.jhazmat.2011.07.034>
- [43] S. Sarkar, C. Bhattacharjee & S. Curcio, Studies on adsorption, reaction mechanisms and kinetics for photocatalytic degradation of CHD, a pharmaceutical waste, *Ecotoxicol Environ Saf.*, 121 (2015) 154-163. <https://doi.org/10.1016/j.ecoenv.2015.04.036>